Radioimmunoscintigraphy and Pretreatment Dosimetry of ^{131}I-Omburtamab for Planning Treatment of Leptomeningeal Disease

Neeta Pandit-Taskar*[1,2], Milan Grkovski*[3], Pat B. Zanzonico[3], Keith S. Pentlow[3], Shakeel Modak[4], Kim Kramer[4], and John L. Humm[3]

[1]*Department of Radiology, Memorial Sloan Kettering Cancer Center, New York, New York;* [2]*Department of Radiology, Weill Cornell Medical College, New York, New York;* [3]*Department of Medical Physics, Memorial Sloan Kettering Cancer Center, New York, New York; and* [4]*Department of Pediatrics, Memorial Sloan Kettering Cancer Center, New York, New York*

Radiolabeled antibody treatment with ^{131}I-omburtamab, administered intraventricularly into the cerebrospinal fluid (CSF) space, can deliver therapeutic absorbed doses to sites of leptomeningeal disease. Assessment of distribution and radiation dosimetry is a key element in optimizing such treatments. Using a theranostic approach, we performed pretreatment ^{131}I-omburtamab imaging and dosimetric analysis in patients before therapy. **Methods:** Whole-body planar images were acquired 3 ± 1, 23 ± 2, and 47 ± 2 h after intracranioventricular administration of 75 ± 5 MBq of ^{131}I-omburtamab via an Ommaya reservoir. Multiple blood samples were also obtained for kinetic analysis. Separate regions of interest (ROIs) were manually drawn to include the lateral ventricles, entire spinal canal CSF space, and over the whole body. Count data in the ROIs were corrected for background and physical decay, converted to activity, and subsequently fitted to an exponential clearance function. The radiation absorbed dose was estimated to the CSF, separately to the spinal column and ventricles, and to the whole body and blood. Biodistribution of the injected radiolabeled antibody was assessed for all patients. **Results:** Ninety-five patients were included in the analysis. Biodistribution showed prompt localization in the ventricles and spinal CSF space with low systemic distribution, noted primarily as hepatic, renal, and bladder activity after the first day. Using ROI analysis, the effective half-lives were 13 ± 11 h (range, 5–75 h) for CSF in the spinal column, 8 ± 3 h (range, 3–17 h) for ventricles, and 41 ± 11 (range, 23–81 h) for the whole body. Mean absorbed doses were 0.63 ± 0.38 cGy/MBq (range, 0.24–2.25 cGy/MBq) for CSF in the spinal column, 1.03 ± 0.69 cGy/MBq (range, 0.27–5.15 cGy/MBq) for the ventricular CSF, and 0.45 ± 0.32 mGy/MBq (range, 0.05–1.43 mGy/MBq) for the whole body. **Conclusion:** Pretherapeutic imaging with ^{131}I-omburtamab allows assessment of biodistribution and dosimetry before the administration of therapeutic activity. Absorbed doses to the CSF compartments and whole body derived from the widely applicable serial ^{131}I-omburtamab planar images had acceptable agreement with previously reported data determined from serial ^{124}I-omburtamab PET scans.

Key Words: antibody; radioimmunotherapy; omburtamab; leptomeningeal; neuroblastoma

J Nucl Med 2023; 64:946–950
DOI: 10.2967/jnumed.122.265131

Several pediatric and adult malignancies, such as leukemia, neuroblastoma, medulloblastoma, and other solid tumors, may metastasize to the central nervous system and present as leptomeningeal disease (*1*). Leptomeningeal disease is difficult to cure and is associated with high morbidity and mortality (*1,2*). Omburtamab is a murine monoclonal antibody that targets glycoprotein antigen B on the cell membrane (B7H3), which is expressed in several cancers, including neuroblastoma (*3*). Intrathecal or intracranioventricular administration of radiolabeled antibodies into the cerebrospinal fluid (CSF) space has been successfully applied by our group and found to be safe and effective for disease control (*4–6*). Previously, we reported on radiation dosimetry and PET imaging with ^{124}I-omburtamab for pretreatment assessment (*7*). However, given the cost and limited availability of ^{124}I, its use was restricted to only a few patients. We used ^{131}I-omburtamab imaging to evaluate the distribution and dosimetry in patients. Here, we present an analysis of pretreatment imaging, including biodistribution and γ-planar imaging-based dosimetry estimates of projected therapeutic absorbed doses for patients who underwent intraventricularly administered ^{131}I-omburtamab therapy. This paper focuses on the results of a dosimetric analysis based on the available pretreatment imaging data.

MATERIALS AND METHODS

Patient Selection

The prospective study was performed under an institutional review board–approved protocol (ClinicalTrials.gov NCT00089245). ^{131}I-omburtamab was administered under U.S. Food and Drug Administration–approved Investigational New Drug application BB-IND 9351. All patients or their legal guardians signed a written informed consent. Patients eligible for treatment under the protocol underwent pretreatment γ-imaging after administration of an ^{131}I-omburtamab dosimetry dose. The study population demographics are presented in Table 1.

^{131}I-Omburtamab Administration

The antibody omburtamab (previously 8H9) was radiolabeled with ^{131}I by Memorial Sloan Kettering Cancer Center's Radiochemistry and Molecular Imaging Probes Core Facility by the method described previously (*6*). ^{131}I-omburtamab was diluted using 1% human serum albumin and filtered using a Millipore (0.2 μm) filter. All patients were assessed for catheter patency and optimal CSF flow to rule out obstruction to CSF flow using the ^{111}In-diethylenetriaminepentaacetic acid CSF flow study. To minimize thyroid uptake, patients were premedicated with oral saturated solution of potassium iodide drops and liothyronine, which was started 5–7 d before administration of ^{131}I-omburtamab. The activity was

Received Nov. 2, 2022; revision accepted Jan. 26, 2023.
For correspondence or reprints, contact Neeta Pandit-Taskar (pandit-n@mkscc.org).
*Contributed equally to this work.
Published online Feb. 9, 2023.

TABLE 1
Subject Demographics and Clinical Characteristics (n = 95)

Characteristic	Patient number (n)
Sex	
Male	53
Female	42
Age at diagnosis (y)	
<5	34
5–10	31
>10	30
Clinical tumor type	
Neuroblastoma	61
Medulloblastoma	13
Ependymoma	5
Metastatic melanoma	2
Pineoblastoma	2
Choroid plexus carcinoma	2
Retinoblastoma	2
Embryonal neuroepithelial tumor	1
Embryonal tumor with neuropil and true rosettes	1
High-grade glioma	1
Metastatic breast carcinoma	1
Metastatic ovarian carcinoma	1
Metastatic sarcoma	1
Primitive neuroectodermal brain tumor	1
Rhabdomyosarcoma	1

administered intraventricularly via Ommaya reservoir access, with the catheter tip terminating in the lateral ventricle.

For pretherapy dosimetry imaging, patients were injected with 75 ± 5 MBq of ^{131}I-omburtamab and serial whole-body γ-camera imaging was performed, which was used to estimate the absorbed dose to the CSF and ventricles. Subsequently, patients received treatment with ^{131}I-omburtamab (activity, 370–2,960 MBq). Posttreatment dosimetric assessment was not performed.

Blood Measurements

Serial peripheral blood samples were obtained, including a baseline sample before injection of the pretherapy imaging dose of ^{131}I-omburtamab and after injection around 15 min, 30 min, 1 h, 2 h, 4–6 h, 18–24 h, and 44–48 h. Samples were weighed and counted in duplicate in the scintillation well counter (LKB Wallac) calibrated for ^{131}I (cpm/MBq), together with the appropriate standard. These data were used to determine the radiolabeled antibody kinetics and dosimetry in blood. The measured count rates were corrected for background count rate and converted to percentage of injected activity per gram, decay-corrected to the time of administration. The following biexponential function was fit to the resulting blood time–activity concentration data using Excel: $Y(t) = A\exp(-\lambda_1 t) + B\exp(-\lambda_2 t)$, where A and B are the 0 time–activity concentrations (in MBq/g), λ_1 and λ_2 are the clearance constants (in 1/h), and t is the time after administration (in h). The function Y(t) was multiplied by the exponential decay factor for ^{131}I (physical half-life, 8.04 d) to yield the decayed time–activity concentration data: $C(t) = Y(t) * \exp^{[-0.693t/(8.04*24)]}$. Integration of this function yields the ^{131}I time-integrated activity concentration; when multiplied by the average energy emitted per decay for ^{131}I β-particles (0.405 g·cGy/μCi·h), it yields the absorbed dose per unit administered activity. These absorbed-dose estimates assume complete local absorption of the ^{131}I β-particles and ignore the small ^{131}I γ-ray dose contribution.

^{131}I-Omburtamab Dosimetry

Whole-body serial planar images were acquired by γ-camera imaging on a Philips Forte (n = 78 patients), Philips/ADAC Vertex (n = 5 patients), Philips Skylight (n = 3 patients), Philips Precedence (n = 4 patients), and GE Discovery 670 (n = 5 patients). Imaging was performed at 3 time points (3 ± 1, 23 ± 2, and 47 ± 2 h) after intraventricular administration of ^{131}I-omburtamab. Planar anterior and posterior images from vertex to pelvis were obtained for all patients at a scan speed of 10 cm/min. All cameras used for imaging (Philips Forte, Vertex, and Skylight cameras and the GE Discovery 670) were equipped with 0.625-in-thick sodium iodide crystals and high-energy collimators. A calibrated ^{131}I standard of ~7.4 MBq was placed alongside the patient for all images.

Regions of interest (ROIs) were manually drawn around the spinal CSF on the posterior image acquired on day 0 and were copied to the anterior image on day 0, as well as to the anterior and posterior images acquired on days 1 and 2 after injection. A separate ROI of equal area was placed 1 to 2 cm to the right of the CSF ROI to estimate the body background activity. The difference in counts between these 2 ROIs provided the net counts within the CSF. Additional ROIs were placed over the ventricles and the whole body on both anterior and posterior images acquired at all 3 time points after injection. Background ROIs were placed adjacent to the ventricles and whole body to estimate background counts. The means were calculated from values obtained on anterior and posterior images. ROI net (background subtracted) geometric mean counts at each time point were converted to activity (in MBq) by dividing by the ^{131}I calibration factor (in counts/MBq).

CSF volume was estimated to be 140 mL, equally distributed between the spinal column and the ventricles. In addition, the CSF volume was scaled based on patient age for younger patients according to the data published by Triarico et al. (*8*). For each ROI, the time–activity data were fit to exponential functions using Excel and the respective functions. The curve was integrated; divided by the CSF, ventricle, and whole-body masses to yield the time-integrated activity concentrations; and multiplied by the equilibrium dose constant for ^{131}I β-particles to yield the respective absorbed doses. First-order attenuation corrections were performed using an ^{131}I linear attenuation coefficient of 0.11 cm^{-1}. For the ventricles, attenuation correction was based on the half-thickness of the measured anterior–posterior dimension of brain on MRI. For CSF, attenuation correction was based on the average CSF depth as measured on MRI sagittal images at the levels of C3, T1, T5, T10, and L4 vertebrae. The normal brain-surface absorbed dose was assumed to be 50% of the absorbed dose to the ventricles. The whole-body attenuation correction was based on the assumption of 10-cm average half-thickness (water equivalent) of the patient in the anterior–posterior direction.

Statistical Analysis

A Mann–Whitney U test for unpaired 2-sample data was used to investigate whether the means for various metrics among different age groups were statistically significant ($P < 0.05$).

RESULTS

Patients

A total of 95 patients (53 male and 42 female; age, 10 ± 11 y; range, 1–54 y) imaged between November 2004 and February 2020 were included in the analysis (Table 1). The average net administered activity of ^{131}I was 75 ± 5 MBq (range, 54–86 MBq). Patients had no severe adverse reactions to the administered activity. Acute side effects were minor, including headache, nausea, or vomiting, which did not vary for 1,850 vs. 2,960 MBq.

Biodistribution

Representative images of patients from different age cohorts are shown in Figure 1. Activity in the Ommaya reservoir at the injection site was not visually discernable (n = 3 patients), minimal or mild (n = 83 patients), or visibly prominent (n = 8 patients) at the first imaging time point and subsequently decreased over 24–48 h. Activity was seen in the fourth ventricle–basal cistern region and CSF canal on day 0 at 2- to 4-h imaging. Distribution along the cerebral hemisphere was noted in all patients: it was seen at 24 h in 77 patients and at 48 h in 18 patients. The uptake was symmetric for 63 patients and mildly asymmetric (differential right vs. left activity noted visually) for the remaining 32 patients. A total of 16 patients exhibited increased uptake in the left side (1 of these patients had photopenia on the right side secondary to surgery), whereas for another 16 patients, increased uptake was noted in the right side of the cerebral hemisphere.

Systemic blood-pool activity was not seen in most patients, except in 5 patients with low-level activity noted at 24–48 h. For kidneys, no discernable uptake was seen in 62 patients at initial imaging, whereas 35 patients showed mild uptake; excreted activity in kidneys and bladder was first noted at 2–4 h, with greater visualization at 24 and 48 h. Activity in the spinal column or CSF was uniformly noted in all patients in the initial images and decreased with time. Thyroid uptake was not visually noted in most patients (n = 91) or was visualized with mild activity at 24- or 48-h imaging in 4 patients. Liver activity was mostly seen at 24–48 h, initially increasing between 2–4 h and 24 h with later stability or slowly decreasing through 48 h. The activity in the liver was only slightly elevated above that background, and in 2 patients, it was not visually discernable. In most patients, there was no splenic uptake (n = 59), whereas mild uptake was noted in some patients (n = 36) that decreased at 48 h. Mild uptake in the stomach was noted in 18 patients at 24 h and in 3 patients at 48 h, with an overall trend of decreasing activity between 24 and 48 h. In 7 patients who had a ventriculoperitoneal shunt, mild uptake was noted in the abdomen and peritoneal region at 24–48 h (Fig. 2). Mild activity in the bones or marrow was noted in 2 patients at 24- to 48-h imaging.

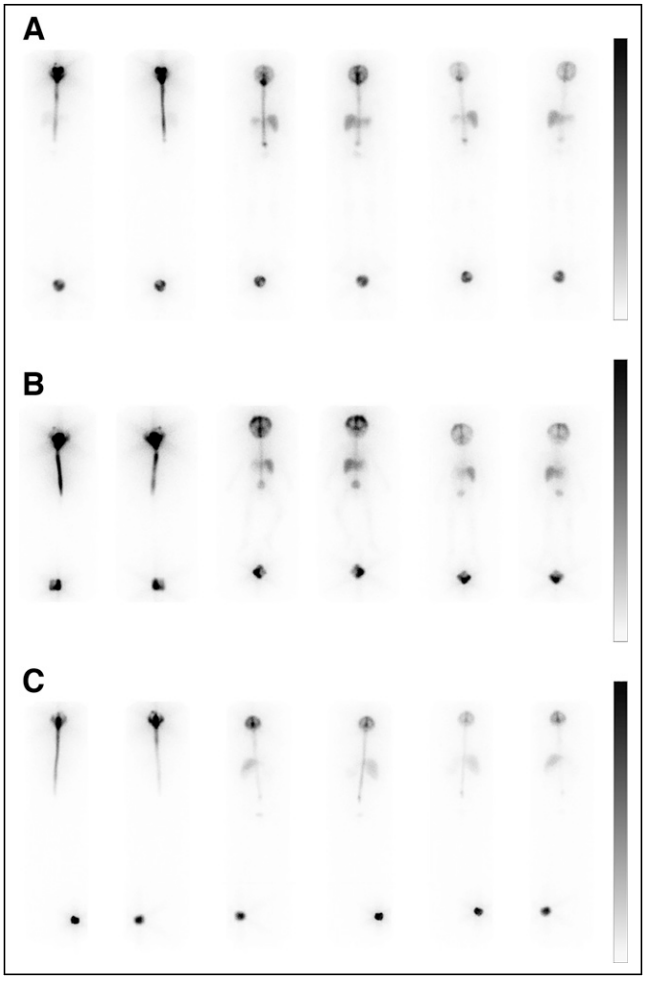

FIGURE 1. Representative planar images of patients from different age subgroups. Displayed scale is 0–100 voxel counts. (A) Anterior (left) and posterior (right) whole-body images of ^{131}I-omburtamab biodistribution at 4, 24, and 48 h. For this patient, calculated absorbed dose was 0.38 cGy/MBq for CSF and 1.36 cGy/MBq for ventricles. Initial standard activity of ^{131}I was 7.5 MBq (200 μCi). (B) Second example patient (1.8 y of age). (C) Third example patient (21 y of age).

Kinetics and Absorbed Doses

Clearance half-times were 13 ± 11 h (range, 5–75 h; median, 9 h) for CSF, 8 ± 3 h (range, 3–17 h; median, 8 h) for ventricles, and 41 ± 11 h (range, 23–81 h; median, 40 h) for the whole body. CSF and ventricle clearance times were significantly higher for the subcohort of patients older than 10 y compared with the subcohort of patients younger than 5 y (Table 2). For <5 y, 5–10 y and >10 y, whole-body clearance times were significantly different for each of the 3 subcohorts (<5, 5–10, and >10 y; Table 2). Whole-body retention at the 3 imaging time points was 74% ± 19%, 59% ± 16%, and 38% ± 12%, respectively (Supplemental Fig. 1) (supplemental materials are available at http://jnm.snmjournals.org). Mean absorbed doses were 0.63 ± 0.38 cGy/MBq (range, 0.24–2.25 cGy/MBq; median, 0.52 cGy/MBq) for CSF, 1.03 ± 0.69 cGy/MBq (range, 0.27–5.15 cGy/MBq; median, 0.83 cGy/MBq) for ventricles, and 0.45 ± 0.32 mGy/MBq (range, 0.05–1.43 mGy/MBq; median, 0.40 mGy/MBq) for the whole body. The CSF mean absorbed dose was higher in the subcohort of patients older than 10 y compared with the subcohort of patients younger than 5 y, whereas the blood absorbed dose was lower (Table 2). No significant differences among the subcohorts were noted for whole-body clearance times. For comparison, the median ^{131}I-omburtamab absorbed doses estimated as projected from ^{124}I-omburtamab PET imaging (*7*) were 0.52 cGy/MBq (CSF), 0.62 cGy/MBq (ventricles), and 0.45 mGy/MBq (whole body).

Effective half-lives and absorbed doses for doses CSF, ventricles, whole body, and blood are summarized in Table 2. The table also includes the corresponding results for the subgroups based on patient age (<5, 5–10, and >10 y). CSF effective half-lives and absorbed doses were significantly higher in patients older than 10 y. No significant difference in ventricle effective half-life or ventricle absorbed dose was observed among the 3 groups. However, significant differences between the oldest subgroup (>10 y) and the other 2 subgroups were observed in blood and whole-body absorbed doses (Table 2).

Blood samples were analyzed in 65 patients. The mean absorbed doses in blood were 0.05 ± 0.05 cGy/MBq (range, 0.003–0.23 cGy/MBq; median, 0.04 cGy/MBq). The mean absorbed doses in the subgroup of patients older than 10 y were significantly lower compared with those for patients in subgroup of patients younger than 5 y and in the 5- to 10-y subgroup (Table 2).

Clinical Follow-up

In phase 1 of the study (ClinicalTrials.gov NCT00089245), 1 instance of dose-limiting toxicity (transient, self-limiting hepatic transaminitis) was encountered. In patients with central nervous system

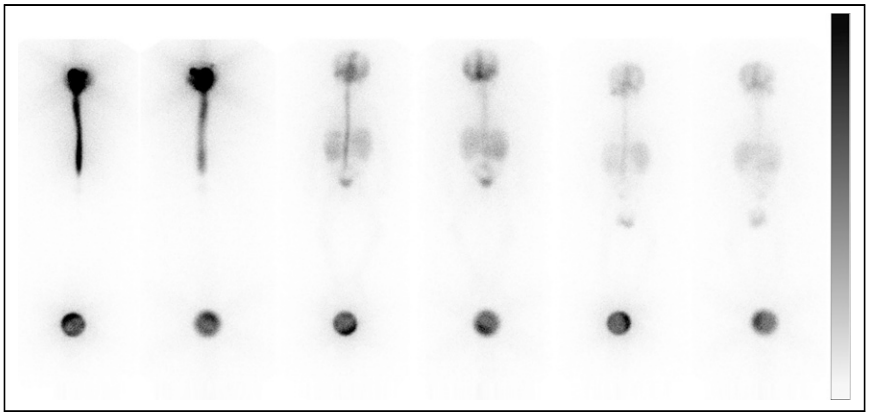

FIGURE 2. Serial anterior and posterior whole-body images of patient with ventriculoperitoneal shunt at 4, 24, and 48 h. For each image, displayed scale is 0–100 voxel counts. Mild uptake is seen in abdomen and peritoneal region at 24–48 h.

relapse of neuroblastoma ($n = 15$) treated with multimodality therapy including ^{131}I-omburtamab, median progression-free survival and overall survival were 7.5 and 11.1 y, respectively. These data are far superior to historical data for patients with central nervous system relapse of neuroblastoma, in whom reported mortality was 100% (*9*). In patients with other nonneuroblastoma diagnoses ($n = 21$), 6 patients survived more than 5 y after radioimmunotherapy, including 2 patients with ependymoma and 1 patient each with medulloblastoma, chordoma, choroid plexus carcinoma, and embryonal tumor with multilayer rosettes (*10*).

DISCUSSION

The results of the current analysis are consistent with our previously published experience with ^{124}I-omburtamab quantitative PET/CT imaging (*7*) in a patient cohort administered pretherapeutic activity of ^{131}I-omburtamab. Compared with ^{124}I-omburtamab PET imaging, ^{131}I-based planar γ-camera imaging is more widely available, more practical, and less expensive than ^{124}I-based dosimetry. However, ^{131}I planar γ-camera imaging-based dosimetry poses several technical challenges for accurate activity quantitation relative to ^{124}I-based PET imaging approaches. For the initial patients in our cohort, SPECT/CT scans could not be performed because such scanners were not available at the time (2004); therefore, only SPECT was performed. The need to anesthetize the younger pediatric patients imposed restrictions on overall scan duration. In the interest of developing a practical scan protocol for this patient population, we performed serial planar whole-body scans at the nominal times of 4, 24, and 48 h after injection and only 1 rapid (20 s/stop) SPECT scan of the head at 24 h.

The intraventricular route of administration allows the delivery of higher therapeutic absorbed-dose ratios to the CSF target volume relative to blood and the whole body. The biodistribution pattern showed good localization and retention into the CSF space, enabling dosing of leptomeningeal disease. The systemic activity distribution was low overall, as expected, with localized delivery of the radiolabeled antibody. The distribution of activity systemically in organs was visually more pronounced at later time points due to systemic absorption and dispersion over time. Activity within the CSF was clearly seen on all 3 serial images. However, the low activity levels within the major organs made our dataset unsuitable for accurate normal organ dosimetry; therefore, the study focused on the feasibility of performing dosimetry to the CSF in the ventricles of the brain and within the spinal column. Rigorous (i.e., pairwise) statistical comparison of the ^{131}I-omburtamab absorbed doses derived by ^{131}I planar imaging and ^{124}I PET imaging was not possible, because individual patients underwent either ^{131}I or ^{124}I pretherapy imaging, not both. Not surprisingly, tissue activities and the resulting absorbed doses were quite variable among patients (e.g., as indicated by the large SD of the mean absorbed doses in Table 2). On average, however, the calculated ^{131}I-omburtamab absorbed doses to the spinal CSF derived from the ^{131}I-omburtamab planar scans were similar (~10%) to the reference standard PET-based method. Larger variation and overestimation (~45%) of the dose to the ventricles only, based on planar γ-scans, was probably related to the placement of ROIs and are similar to our previously published ^{124}I-omburtamab PET data (*7*). Recognizing that quantitation of tissue activity by ^{124}I PET (with 3-dimensional images

TABLE 2
Dosimetry for CSF and Ventricles After Intracranioventricular Administration of ^{131}I-Omburtamab in 95 Patients

	CSF		Ventricles			Whole body	
Age group	Absorbed dose (cGy/MBq)	Clearance (h)	Absorbed dose (cGy/MBq)	Clearance (h)	Blood* (absorbed dose [mGy/MBq])	Absorbed dose (mGy/MBq)	Clearance (h)
<5 y, $n = 34$	0.50 ± 0.18 (0.29–1.12)	10.6 ± 11.7 (5.8–74.6)	1.13 ± 0.96 (0.30–5.15)	7.0 ± 2.3 (3.4–14.0)	0.63 ± 0.37 (0.12–1.57)	0.67 ± 0.31 (0.07–1.41)	41.2 ± 10.2 (25.2–65.0)
5–10 y, $n = 31$	0.52 ± 0.21 (0.24–1.06)	9.4 ± 2.9 (5.5–19.2)	1.01 ± 0.55 (0.38–2.47)	8.0 ± 3.0 (3.8–15.7)	0.67 ± 0.54 (0.10–2.30)	0.46 ± 0.26† (0.05–1.43)	40.6 ± 7.5 (25.8–61.0)
>10 y, $n = 30$	0.90 ± 0.52† (0.24–2.25)	19.1 ± 13.2† (7.8–57.8)	0.95 ± 0.41 (0.27–1.92)	8.3 ± 2.7† (4.3–17.2)	0.30 ± 0.40† (0.03–1.45	0.20 ± 0.16† (0.05–0.66)	42.3 ± 14.3 (22.6–80.8)
All, $n = 95$*	0.63 ± 0.38 (0.24–2.25)	13.0 ± 10.9 (5.5–74.6)	1.03 ± 0.69 (0.27–5.15)	7.7 ± 2.6 (3.4–17.2)	0.54 ± 0.46 (0.03–2.30)	0.45 ± 0.32 (0.05–1.43)	41.3 ± 10.9 (22.6–80.8)

*Blood data were available for $n = 24$, 20, and 21 patients in 3 age groups.
†Significant difference with respect to <5-y group based on Mann–Whitney *U* test for unpaired 2-sample data.
Data are median and range.

and accurate scatter and attenuation corrections) is considerably more accurate than that of ^{131}I planar scanning (with 2-dimensional images, first-order attenuation correction, and no scatter correction), the better-than-50% agreement on average between the ^{131}I- and the ^{124}I-derived absorbed-dose estimates is reasonable. The closer dosimetry agreement for the CSF within spine is likely due to its simpler geometry and greater distance from the Ommaya reservoir injection site. In addition, an important contributing factor to this discrepancy is that PET provides a direct measure of the activity per unit volume (in MBq/cc), whereas quantitative planar images can provide accurate information about the activity but not the volume of distribution in which the activity resides. These dosimetry-based estimates for administered activity were well within the designated limits of safety for normal organs. The absorbed dose to the CSF compartment was high with very low background uptake in the remainder of the body, yielding a 10-fold-higher absorbed dose to the CSF space than to the whole body (mean, 0.045 cGy/MBq). None of the patients were noted to have normal-organ toxicities involving lung, liver, kidney, or marrow. Blood estimates showed a large margin of safety as well for the activity administered in patients. Based on the absorbed-dose estimates to blood, approximately 3,700 MBq of ^{131}I-omburtamab can be administered before exceeding a maximum tolerated blood dose of 200 cGy; this administered activity threshold is well above the actual treatment activities of 1,850–2,960 MBq given intraventricularly. This reflects a high therapeutic index that can be achieved using intraventricular administration. This is supported by the finding of no significant marrow toxicity in these patients resulting from the treatment doses (*6*). There was no difference in whole-body clearance half-times (40–42 h) among age groups, yielding higher whole-body absorbed doses to younger patients as a consequence of their lower body mass (Table 2).

The limitations of the study include the use of planar imaging only and the lack of late imaging time points. Most included patients (84 of 95) were younger than 18 y, with 34 patients younger than 5 y. In principle, increasing the number of scans would have increased the accuracy of the dosimetric calculations, yet performing more than 3 scans more than 48 h after injection would have considerably increased the complexity of the acquisition and was a practical restriction in patients, especially those requiring anesthesia. An additional limitation is that only planar imaging was performed; that is, SPECT imaging was not performed in all patients. Thus, direct comparison between values obtained from planar images and those obtained from SPECT images was not possible for individual patients. Instead, populationwise dosimetric assessments as derived from planar scans were compared with those derived from fully quantitative ^{124}I-based PET.

However, this study delineates the feasibility of planar imaging using a tracer dose of ^{131}I-omburtamab. Because ^{131}I is more widely available and cheaper than ^{124}I, the use of ^{131}I-omburtamab planar imaging offers a practical alternative to theranostic dosimetry estimation. A multicenter phase 2/3 clinical trial (ClinicalTrials.gov NCT03275402) was recently completed. Further data from this completed study will help validate the use of ^{131}I-omburtamab and facilitate efforts to make this widely available for clinical use.

CONCLUSION

In this study, we demonstrate the feasibility of performing dosimetric assessments with ^{131}I-omburtamab for estimation of the absorbed dose to the CSF compartment in patients who will receive ^{131}I-omburtamab therapy. The results show acceptable agreement between dosimetry estimates performed using serial whole-body planar γ-camera imaging and those from ^{124}I-based PET imaging.

DISCLOSURE

This study was funded by a Department of Radiology Seed Grant of Memorial Sloan Kettering Cancer Center (MSK), with support from MSK's Radiochemistry & Molecular Imaging Probes Core, supported in part through NIH/NCI Cancer Center support grant P30 CA008748. Neeta Pandit-Taskar has served as a consultant or advisory board member for or received honoraria from Actinium Pharma, Progenics, Medimmune/AstraZeneca, Illumina, and ImaginAb and conducts research institutionally supported by Y-mAbs Therapeutics, ImaginAb, BMS, Bayer, Clarity Pharma, Janssen, and Regeneron. Kim Kramer received support from NIH grants K08 CA072868, R21 CA089935, and R21 CA117076, as well as grant support from Luke's Lollies and Catie Find a Cure. Pat Zanzonico serves or has served as a consultant to and received honoraria from Novartis and Radionetics and has licensed intellectual property to Y-mAbs. Milan Grkovski received support from Y-mAbs. No other potential conflict of interest relevant to this article was reported.

KEY POINTS

QUESTION: What are the dosimetry estimates for intraventricular administration of ^{131}I-omburtamab?

PERTINENT FINDINGS: Localized delivery of therapeutic antibody delivers high radiation doses to the CSF compartment with minimal systemic distribution and low doses to normal organs. The biodistribution and radiation dosimetry estimates could be reliably obtained with ^{131}I-omburtamab.

IMPLICATIONS FOR PATIENT CARE: ^{131}I-omburtamab–based dosimetry is a feasible option that allows estimation of biodistribution and radiation dose in patients before treatment. The results are comparable to those of ^{124}I-omburtamab imaging.

REFERENCES

1. Kramer K, Kushner B, Heller G, Cheung NK. Neuroblastoma metastatic to the central nervous system. The Memorial Sloan-Kettering Cancer Center experience and a literature review. *Cancer.* 2001;91:1510–1519.
2. Kramer K, Kushner BH, Cheung NK. Oral topotecan for refractory and relapsed neuroblastoma: a retrospective analysis. *J Pediatr Hematol Oncol.* 2003;25:601–605.
3. Modak S, Kramer K, Gultekin SH, Guo HF, Cheung NK. Monoclonal antibody 8H9 targets a novel cell surface antigen expressed by a wide spectrum of human solid tumors. *Cancer Res.* 2001;61:4048–4054.
4. Kramer K, Cheung NK, Humm JL, et al. Targeted radioimmunotherapy for leptomeningeal cancer using (131)I-3F8. *Med Pediatr Oncol.* 2000;35:716–718.
5. Kramer K, Humm JL, Souweidane MM, et al. Phase I study of targeted radioimmunotherapy for leptomeningeal cancers using intra-Ommaya 131-I-3F8. *J Clin Oncol.* 2007;25:5465–5470.
6. Kramer K, Kushner BH, Modak S, et al. Compartmental intrathecal radioimmunotherapy: results for treatment for metastatic CNS neuroblastoma. *J Neurooncol.* 2010;97:409–418.
7. Pandit-Taskar N, Zanzonico PB, Kramer K, et al. Biodistribution and dosimetry of intraventricularly administered (124)I-omburtamab in patients with metastatic leptomeningeal tumors. *J Nucl Med.* 2019;60:1794–1801.
8. Triarico S, Maurizi P, Mastrangelo S, Attinà G, Capozza MA, Ruggiero A. Improving the brain delivery of chemotherapeutic drugs in childhood brain tumors. *Cancers (Basel).* 2019;11:824.
9. Matthay KK, Brisse H, Couanet D, et al. Central nervous system metastases in neuroblastoma: radiologic, clinical, and biologic features in 23 patients. *Cancer.* 2003;98:155–165.
10. Kramer K, Pandit-Taskar N, Kushner BH, et al. Phase 1 study of intraventricular ^{131}I-omburtamab targeting B7H3 (CD276)-expressing CNS malignancies. *J Hematol Oncol.* 2022;15:165.